International Journal of Solids and Structures 46 (2009) 4038–4053

Contents lists available at ScienceDirect

International Journal of Solids and Structures

journal homepage: www.elsevier.com/locate/ijsolstr

Sliding frictional contact between a rigid punch and a laterally graded elastic medium

Serkan Dag [a,*], Mehmet A. Guler [b], Bora Yildirim [c], A. Cihan Ozatag [a]

[a] Department of Mechanical Engineering, Middle East Technical University, Ankara 06531, Turkey
[b] Department of Mechanical Engineering, TOBB University of Economics and Technology, Ankara 06560, Turkey
[c] Department of Mechanical Engineering, Hacettepe University, Ankara 06800, Turkey

ARTICLE INFO

Article history:
Received 14 May 2009
Received in revised form 20 July 2009
Available online 4 August 2009

Keywords:
Laterally graded materials
Sliding contact
Singular integral equations
Finite element method
Contact stresses

ABSTRACT

Analytical and computational methods are developed for contact mechanics analysis of functionally graded materials (FGMs) that possess elastic gradation in the lateral direction. In the analytical formulation, the problem of a laterally graded half-plane in sliding frictional contact with a rigid punch of an arbitrary profile is considered. The governing partial differential equations and the boundary conditions of the problem are satisfied through the use of Fourier transformation. The problem is then reduced to a singular integral equation of the second kind which is solved numerically by using an expansion–collocation technique. Computational studies of the sliding contact problems of laterally graded materials are conducted by means of the finite element method. In the finite element analyses, the laterally graded half-plane is discretized by quadratic finite elements for which the material parameters are specified at the centroids. Flat and triangular punch profiles are considered in the parametric analyses. The comparisons of the results generated by the analytical technique to those computed by the finite element method demonstrate the high level of accuracy attained by both methods. The presented numerical results illustrate the influences of the lateral nonhomogeneity and the coefficient of friction on the contact stresses.

1. Introduction

Functionally graded materials (FGMs) are multiphase composites that possess smooth spatial variations in the volume fractions of the constituent phases. This broad definition encompasses a wide variety of materials which have gradations in their mechanical, thermal, optical or electrical properties (Khor and Gu, 2000; Park et al., 2000; Cannillo et al., 2007; Yang and Xiang, 2007). In the last decade, the FGM concept has proved to be useful in processing new materials with improved tribological performance. Both experimental and theoretical studies are conducted to examine the feasibility of using FGMs in tribological applications, which generally demand resistance to contact related damage. These studies show that utilization of FGM surfaces in tribological applications leads to improvements in wear resistance (Yue and Li, 2008; Zhang et al., 2008). Furthermore, a controlled gradient in the modulus of elasticity at a surface is shown to eliminate conical cracking that results from Hertzian indentation (Jitcharoen et al., 1998; Pender et al., 2001a,b) and suppress the formation of herringbone cracks under sliding frictional contact (Suresh et al., 1999). The improved tribological characteristics of FGMs paved the way for their potential use in technological applications such as joint prostheses (Mishina et al., 2008) and high performance cutting tools (Nomura et al., 1999).

In the technical literature, various methods, geometries and loading conditions are considered in the contact mechanics analyses of functionally graded materials. Giannakopoulos and Pallot (2000) provided analytical closed form solutions for the two dimensional contact of rigid cylinders on graded elastic substrates. When it is not possible to derive analytical closed form solutions for a contact mechanics problem, generally the problem is reduced to a singular integral equation (SIE) which is solved numerically to compute the required quantities. Dag and Erdogan (2002a) proposed such an SIE based technique to examine the behavior of a surface crack located in an FGM half-plane that is loaded through a frictional flat stamp. Numerical results illustrating the behavior of a surface crack at an FGM surface loaded by a circular stamp are given by the same authors (Dag and Erdogan, 2002b). Guler and Erdogan (2004, 2006, 2007) considered various two dimensional sliding frictional contact problems of FGM coatings by using the singular integral equations. In a series of articles, Ke and Wang developed SIE based solution techniques for two dimensional sliding frictional contact problems of FGMs with arbitrarily varying elastic properties (Ke and Wang, 2006, 2007a) and for partial slip contact problems of FGMs (Ke and Wang, 2007b,c). Yang and Ke

* Corresponding author. Tel.: +90 312 2102580; fax: +90 312 2102536.
E-mail address: sdag@metu.edu.tr (S. Dag).

0020-7683/$ - see front matter © 2009 Elsevier Ltd. All rights reserved.
doi:10.1016/j.ijsolstr.2009.07.023

(2008) studied a two dimensional contact problem for a coating-graded layer–substrate structure loaded by a rigid cylindrical punch. Choi and Paulino (2008) detailed a method based on the singular integral equations which takes into account the effect of frictional heat generation on the contact stress distributions in problems involving FGM coatings and interlayers. Guler (2008) outlined an analytical procedure for the solution of contact problems of thin films and cover plates that are bonded to functionally graded substrates.

In all the studies mentioned in the foregoing paragraph, the material property gradation of the functionally graded medium is assumed to be in the thickness direction and perpendicular to the contact surface. However, in certain technological applications, components that have material property gradations in the lateral direction instead of the thickness direction could also be useful in improving various characteristics of the system behavior. As an example, we consider the bone plates which are used in contact with bones in order to immobilize the fractured segments. It is shown that a bone plate with a lateral gradient in its modulus of elasticity causes less stress-shielding in the bone which facilitates callus formation and improves the bone healing characteristics (Ganesh et al., 2005). The objective in the present study is to develop analytical and computational methods for contact mechanics analysis of functionally graded materials that possess material property gradation in the lateral direction. In the analytical approach, we consider an FGM half-plane in sliding frictional contact with a rigid punch of an arbitrary profile. The shear modulus of the half-plane is assumed to vary exponentially along the lateral direction. The direction of the material property gradation is taken to be perpendicular to the normal of the contact surface. The problem is reduced to a singular integral equation of the second kind which is solved numerically to compute the contact stress distributions. In order to provide more insight into the behavior of the functionally graded materials with lateral gradation, contact mechanics analysis is also conducted by means of the finite element method. This dual approach methodology allows a direct comparison between the analytical and computational results leading to a highly accurate predictive capability. The parametric analyses are performed by considering flat and triangular punch profiles, the former being representative of a complete contact problem and the latter of an incomplete contact problem. The presented results illustrate the influences of the lateral nonhomogeneity and the coefficient of Coulomb friction on the distributions of the contact stresses.

2. Analytical solution

The geometry of the considered contact mechanics problem is depicted in Fig. 1. A functionally graded elastic half-plane is in sliding frictional contact with a rigid punch of an arbitrary profile. The contact area extends from $y = a$ to $y = b$ at the surface $x = 0$. Coulomb's dry friction law is assumed to hold in the contact area hence the tangential force per unit length Q transferred by the contact is taken to be equal to ηP where η is the coefficient of friction and P is the applied normal force per unit length. The shear modulus of the graded medium varies in the lateral direction, i.e. in y-direction. This variation is represented by an exponential function in the following form:

$$\mu(y) = \mu_0 \exp(\gamma y), \tag{1}$$

where μ_0 is the value of the shear modulus at $y = 0$ and γ is a nonhomogeneity constant. The spatial variation of the Poisson's ratio is assumed to be negligible. As a result, the Poisson's ratio v is considered to be a constant. Under these assumptions, the equations of equilibrium in terms of the displacement components are obtained as follows:

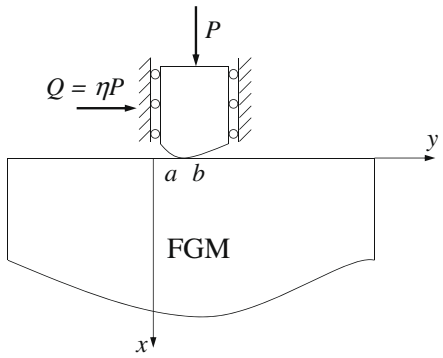

Fig. 1. An FGM half-plane in frictional sliding contact with a rigid punch of an arbitrary profile.

$$(\kappa+1)\frac{\partial^2 u}{\partial x^2} + (\kappa-1)\frac{\partial^2 u}{\partial y^2} + 2\frac{\partial^2 v}{\partial x \partial y} + \gamma(\kappa-1)\frac{\partial u}{\partial y} + \gamma(\kappa-1)\frac{\partial v}{\partial x} = 0, \tag{2}$$

$$(\kappa+1)\frac{\partial^2 v}{\partial y^2} + (\kappa-1)\frac{\partial^2 v}{\partial x^2} + 2\frac{\partial^2 u}{\partial x \partial y} + \gamma(\kappa+1)\frac{\partial v}{\partial y} + \gamma(3-\kappa)\frac{\partial u}{\partial x} = 0, \tag{3}$$

where u and v are the displacement components in x- and y-directions, respectively, $\kappa = 3 - 4v$ for plane strain and $\kappa = (3 - v)/(1 + v)$ for plane stress.

The contact mechanics problem defined above has to be solved by considering the following mixed boundary conditions:

$$\sigma_{xx}(0,y) = \sigma_{xy}(0,y) = 0, \quad -\infty < y < a, \quad b < y < \infty, \tag{4}$$

$$\sigma_{xx}(0,y) = p(y), \quad \sigma_{xy}(0,y) = \eta p(y), \quad a < y < b, \tag{5}$$

$$\frac{\partial u(0,y)}{\partial y} = f(y), \quad a < y < b, \tag{6}$$

$$\int_a^b \sigma_{xx}(0,y)dy = -P, \tag{7}$$

where $p(y)$ is the primary unknown function of the formulation which stands for the contact stress and $f(y)$ is a known function dictated by the profile of the rigid punch. In addition, the solution of the problem must satisfy the regularity conditions at infinity, requiring that all field quantities should be bounded as $(x^2 + y^2) \to \infty$.

The general solutions for the displacement and stress components are obtained by applying Fourier transformation to Eqs. (2) and (3) in y-direction. After applying the Fourier transforms and solving the resulting system of ordinary differential equations, the displacement components are found as

$$u(x,y) = \frac{1}{2\pi}\int_{-\infty}^{\infty}\sum_{j=1}^{2} M_j(\rho)\exp(s_j x + i\rho y)d\rho, \tag{8}$$

$$v(x,y) = \frac{1}{2\pi}\int_{-\infty}^{\infty}\sum_{j=1}^{2} M_j(\rho)N_j\exp(s_j x + i\rho y)d\rho, \tag{9}$$

where $M_j(\rho)$ $(j = 1,2)$ are unknown functions of ρ, i stands for the imaginary unit $\sqrt{-1}$ and s_j and N_j $(j = 1,2)$ are given as follows:

$$s_1 = -\frac{1}{2}\gamma\sqrt{\frac{3-\kappa}{\kappa+1}} - \frac{1}{2}\sqrt{4\rho^2 + 4i\gamma\rho + \gamma^2\frac{3-\kappa}{\kappa+1}}, \quad \Re(s_1) < 0, \tag{10}$$

$$s_2 = \frac{1}{2}\gamma\sqrt{\frac{3-\kappa}{\kappa+1}} - \frac{1}{2}\sqrt{4\rho^2 + 4i\gamma\rho + \gamma^2\frac{3-\kappa}{\kappa+1}}, \quad \Re(s_2) < 0, \tag{11}$$

$$N_j = -\frac{(\kappa+1)s_j^2 + \gamma(\kappa-1)i\rho - (\kappa-1)\rho^2}{\{2i\rho + \gamma(\kappa-1)\}s_j}, \quad (j = 1,2). \tag{12}$$

The general solutions for the in-plane stress components σ_{xx}, σ_{xy} and σ_{yy} are derived by using Eqs. (8) and (9) and Hooke's Law.

The boundary conditions given by Eqs. (4) and (5) are imposed on the general solutions so as to express $M_1(\rho)$ and $M_2(\rho)$ in terms of $p(y)$. The following linear system is obtained by using Eqs. (4) and (5)

$$\begin{bmatrix} s_1(\kappa+1)+i\rho(3-\kappa) & s_2(\kappa+1)+i\rho(3-\kappa) \\ i\rho+N_1 s_1 & i\rho+N_2 s_2 \end{bmatrix} \begin{bmatrix} M_1(\rho) \\ M_2(\rho) \end{bmatrix} = \begin{bmatrix} (\kappa-1)\int_a^b \frac{p(t)}{\mu(t)}\exp(-i\rho t)dt \\ \eta\int_a^b \frac{p(t)}{\mu(t)}\exp(-i\rho t)dt \end{bmatrix}. \tag{13}$$

The solution of this linear system reads as follows:

$$M_j(\rho) = \phi_j(\rho)\int_a^b \frac{p(t)}{\mu(t)}\exp(-i\rho t)dt + \eta\lambda_j(\rho) \times \int_a^b \frac{p(t)}{\mu(t)}\exp(-i\rho t)dt \quad (j=1,2). \tag{14}$$

The functions $\phi_j(\rho)$ and $\lambda_j(\rho)$ $(j=1,2)$ are determined by making use of the symbolic manipulator MAPLE.

The singular integral equation is derived by using the condition (6) and Eqs. (8) and (14). In the derivation of the singular integral equation, asymptotic analyses are required to be conducted for the extraction of the dominant singular terms. After conducting the required asymptotic analyses, the singular integral equation, which is of the second kind, is obtained in the following form:

$$\frac{1}{\pi}\int_a^b \frac{P_1(t)}{y-t}dt - \eta\frac{\kappa-1}{\kappa+1}P_1(y) + \frac{2}{\pi(\kappa+1)}\int_a^b \{k_1(y,t) + \eta k_2(y,t)\}P_1(t)dt = \frac{4\mu_0}{\kappa+1}f(y), \quad a<y<b. \tag{15}$$

The unknown function of the integral equation, i.e. $P_1(y)$, is related to the contact stress as

$$P_1(y) = \exp(-\gamma y)p(y), \quad a<y<b. \tag{16}$$

The procedure of conducting asymptotic analysis for the extraction of the singular terms is described in various sources. The reader may refer to the paper by Guler and Erdogan (2004) for further details on the derivation of the dominant singular terms of integral equations. The expressions of the functions $k_1(y,t)$ and $k_2(y,t)$ in Eq. (15) are given in Appendix A.

A numerical solution procedure based on the expansion–collocation method is developed so as to solve the singular integral equation (Eq. (15)) in conjunction with the equilibrium condition given by Eq. (7). The numerical solution is carried out by considering both complete and incomplete contact problems. In a complete contact problem, the size of the contact area is independent of the applied contact force whereas in an incomplete contact the size of the contact area is strongly dependent upon the applied force (Hills and Nowell, 1994). In the present study, numerical results are generated for flat and triangular punches, the former being representative of the complete contact problem and the latter of the incomplete contact problem. The geometries of the punch profiles are depicted in Fig. 2. The flat punch has sharp corners at $y=a$ and $y=b$. Hence, the contact stress $p(y)$ is singular at both of those points. In the case of the triangular punch, there is a sharp corner at $y=a$ and there is smooth contact at $y=b$. Therefore, for the triangular punch, $p(y)$ is singular at $y=a$ and zero at $y=b$. The angle of inclination of the triangular punch is denoted by θ.

In order to numerically solve the singular integral equation, we first introduce the following definitions:

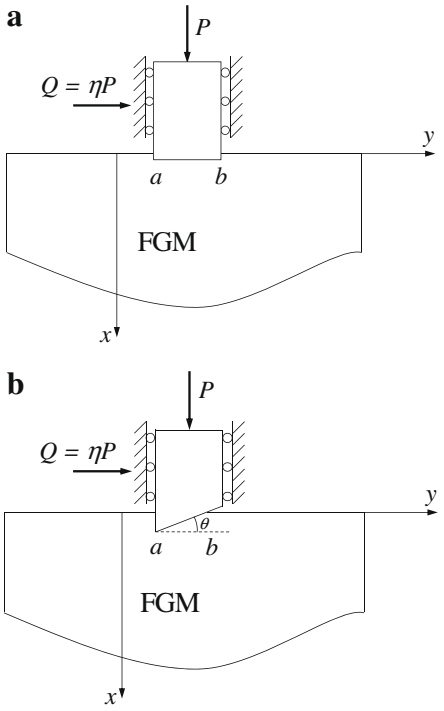

Fig. 2. The geometries of the punch problems considered: (a) flat punch; (b) triangular punch.

$$y = \frac{b-a}{2}s + \frac{b+a}{2}, \quad a<y<b, \quad -1<s<1, \tag{17}$$

$$t = \frac{b-a}{2}r + \frac{b+a}{2}, \quad a<t<b, \quad -1<r<1, \tag{18}$$

$$P_1(y) = P_1\left(\frac{b-a}{2}s + \frac{b+a}{2}\right) = \widetilde{P}_1(s). \tag{19}$$

For both flat and triangular punches, the normalized forms of the singular integral equation and the equilibrium condition are then expressed as follows:

$$\frac{1}{\pi}\int_{-1}^{1}\frac{\overline{P}_1(r)dr}{s-r} - \eta\frac{\kappa-1}{\kappa+1}\overline{P}_1(s) + \frac{(b-a)}{\pi(\kappa+1)}\int_{-1}^{1}\{\tilde{k}_1(s,r)+\eta\tilde{k}_2(s,r)\}\overline{P}_1(r)dr = -\frac{4}{\kappa+1}R, \quad -1<s<1, \tag{20}$$

$$\int_{-1}^{1}\overline{P}_1(r)\exp\left\{\frac{\gamma}{2}((b-a)r+(b+a))\right\}dr = -g, \quad -1<s<1, \tag{21}$$

where

$$\tilde{k}_j(s,r) = k_j\left(\frac{b-a}{2}s + \frac{b+a}{2}, \frac{b-a}{2}r + \frac{b+a}{2}\right) \quad (j=1,2). \tag{22}$$

$\overline{P}_1(r)$, R and g all depend on the particular type of the punch profile considered and are defined as given below:

$$\overline{P}_1(r) = \begin{cases} \frac{\widetilde{P}_1(r)}{P/(b-a)} & \text{for the flat punch,} \\ \frac{\widetilde{P}_1(r)}{\mu_0\tan(\theta)} & \text{for the triangular punch,} \end{cases} \tag{23}$$

$$R = \begin{cases} 0 & \text{for the flat punch,} \\ 1 & \text{for the triangular punch,} \end{cases} \tag{24}$$

$$g = \begin{cases} 2 & \text{for the flat punch,} \\ \frac{2P}{\mu_0\tan(\theta)(b-a)} & \text{for the triangular punch.} \end{cases} \tag{25}$$

The singular behavior of the unknown function $\overline{P}_1(r)$ in Eq. (20) can be determined through a function-theoretic analysis as described by Erdogan (1978). After determining the singular behavior of the

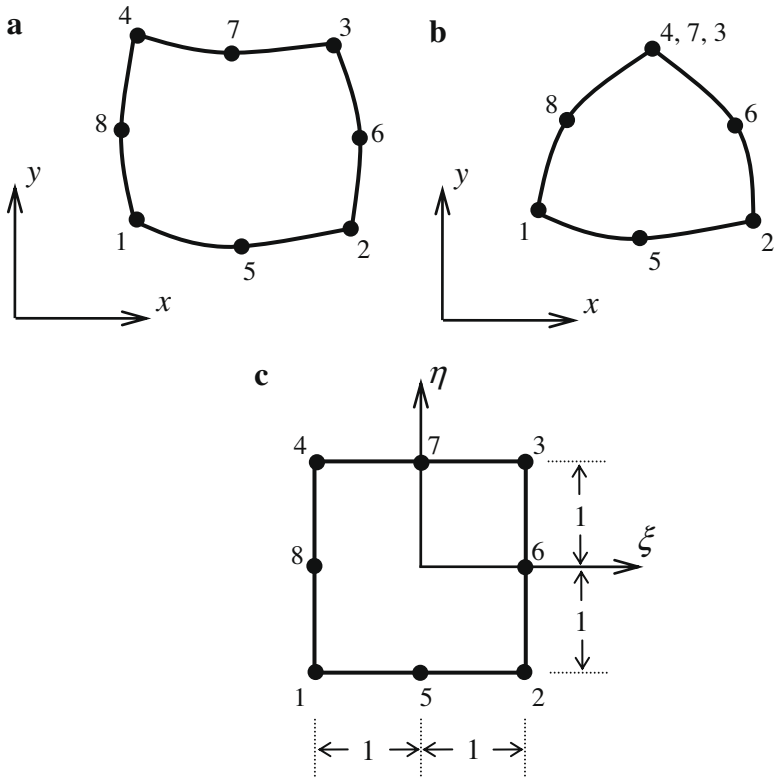

Fig. 3. (a) The quadrilateral finite element in the global coordinate system; (b) the triangular finite element in the global coordinate system; (c) the quadrilateral and the triangular finite elements in the isoparametric coordinate system.

solution, it is possible to express $\overline{P}_1(r)$ as an infinite series in terms of the Jacobi polynomials for both flat and triangular punch problems. The series representation of $\overline{P}_1(r)$ can be written in the following way:

$$\overline{P}_1(r) = (1-r)^{\beta_1}(1+r)^{\beta_2}\left\{\sum_{n=0}^{\infty} A_n P_n^{(\beta_1,\beta_2)}(r)\right\}, \quad -1 < r < 1, \tag{26}$$

where A_n's are unknown constants and $P_n^{(\beta_1,\beta_2)}$ is the Jacobi polynomial of order n. β_1 and β_2 stand for the strengths of the singularities at the end points $y = b$ and $y = a$, respectively. The expressions for these exponents are derived through the function-theoretic analysis and given as follows:

$$\beta_1 = \frac{1}{\pi}\operatorname{arc\,cot}\left(-\eta\frac{\kappa-1}{\kappa+1}\right), \quad \beta_2 = \frac{1}{\pi}\operatorname{arc\,cot}\left(\eta\frac{\kappa-1}{\kappa+1}\right). \tag{27}$$

β_1 and β_2 should be selected such that $-1 < \beta_1 < 0$ and $-1 < \beta_2 < 0$ for the flat punch and $0 < \beta_1 < 1$ and $-1 < \beta_2 < 0$ for the triangular punch. The strengths of the singularities given above are identical to those derived for a homogeneous medium (Dag and Erdogan, 2002a; Ozatag, 2003; Guler and Erdogan, 2004). Hence, it can be concluded that the singular behavior of the contact stress is not affected by a continuous gradation in the lateral direction. In the numerical solution, the infinite series given by Eq. (26) is truncated at $n = N$. The truncated form is substituted into Eqs. (20) and (21). The singular integral equation is then regularized by following the method out-

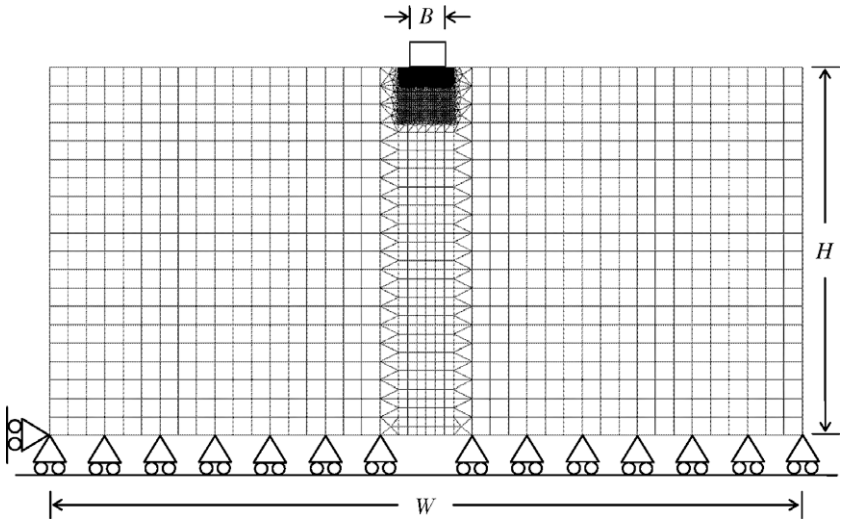

Fig. 4. The finite element mesh used in the analysis of the flat punch problem.

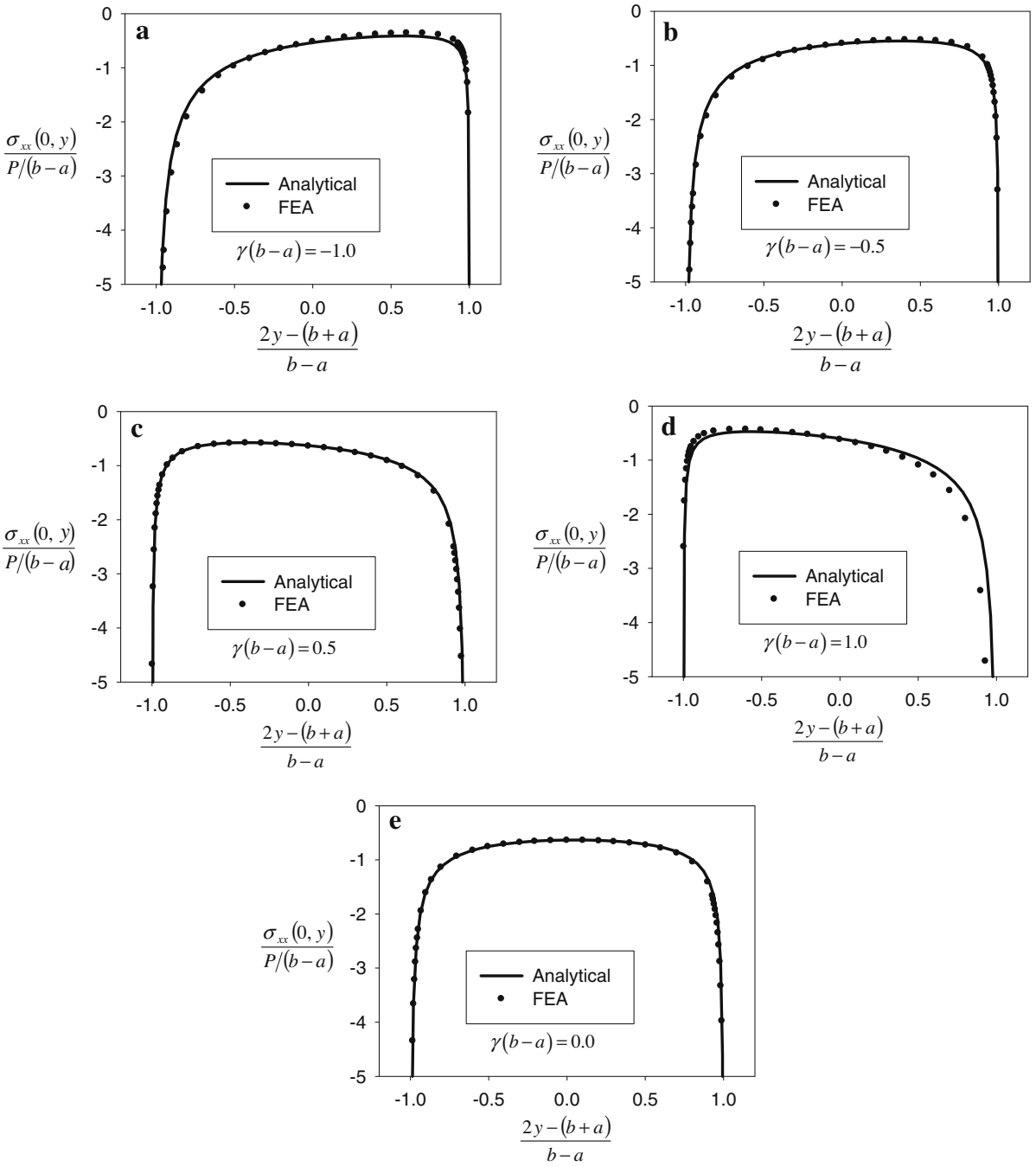

Fig. 5. Comparisons of the normalized contact stress distributions generated by considering a flat punch: (a) $\gamma(b-a)=-1.0$; (b) $\gamma(b-a)=-0.5$; (c) $\gamma(b-a)=0.5$; (d) $\gamma(b-a)=1.0$; (e) $\gamma(b-a)=0.0$. $\eta=0.3,\ \gamma(b+a)=0,\ \kappa=1.8$.

lined by Erdogan (1978). A collocation approach is used to convert Eqs. (20) and (21) into a system of linear algebraic equations in terms of the coefficients of the N^{th} partial sum $A_n\ (n=0,\ldots,N)$.

Note that the length of the contact region $(b-a)$ is independent of the applied force P in the case of the flat punch whereas it is strongly dependent upon P for the triangular punch. As a result, slightly different numerical solution strategies are needed for the flat and triangular punch problems. In the case of the flat punch, a total of $(N+1)$ linear equations are obtained by collocating Eq. (20) at N points and by using Eq. (21). These $(N+1)$ equations are solved simultaneously to calculate $A_n\ (n=0,\ldots,N)$. For the triangular punch however, Eq. (20) is collocated at $(N+1)$ points and the resulting system of $(N+1)$ equations is solved to compute A_n's. The calculated values of $A_n\ (n=0,\ldots,N)$ are then substituted into Eq. (21) so as to calculate the quantity $P/(\mu_0\tan(\theta)(b-a))$ (see Eq. (25)). Hence, for the triangular punch, a relationship between the contact force P and the length of the contact region $(b-a)$ is obtained in terms of μ_0 and the punch inclination angle θ. For both the flat and the triangular punch problems once the A_n's are determined, the normalized contact stress distribution can be calculated by using the truncated form of Eq. (26).

3. Computational approach

In addition to the analytical technique described in the previous section, a computational approach based on the finite element

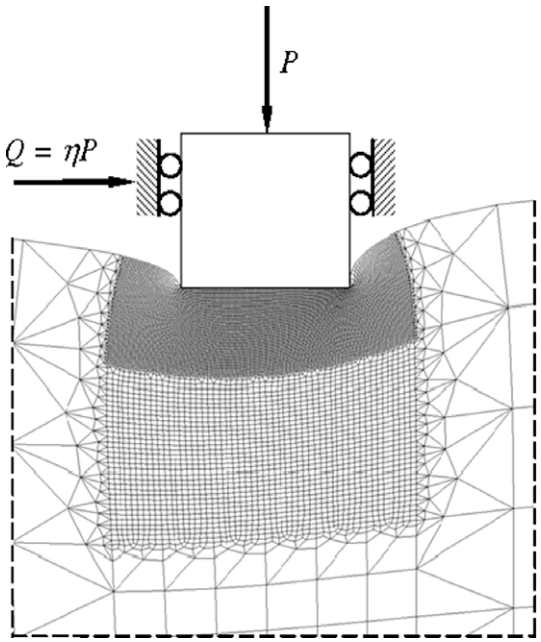

Fig. 6. Deformed shape of the finite element mesh of the region around the contact zone generated by considering a flat punch, $\eta=0.3, \gamma(b+a)=0, \kappa=1.8, \gamma(b-a)=0.5$.

method is also used to study contact mechanics problems of FGMs that possess elastic gradation in the lateral direction. The primary advantage of this dual approach methodology is that it permits direct comparisons between analytical and computational results, leading to the development of a reliable numerical predictive capability. The finite element analyses are conducted by using the general purpose finite element analysis software ANSYS (1997). Finite element models are developed to study the contact mechanics problems of flat and triangular punches which are illustrated by Fig. 2. The functionally graded medium outside the contact zone is discretized by using 8-noded quadrilateral and 6-noded triangular elements. The 6-noded triangle is formed in ANSYS by merging the three nodes of an 8-noded quadrilateral element at a single point. The quadrilateral and the triangular elements in the global and the isoparametric coordinate systems are shown in Fig. 3. In the contact zone, contact line elements are utilized in the discretization of the functionally graded medium. The rigid flat and triangular punches are represented by rigid target elements.

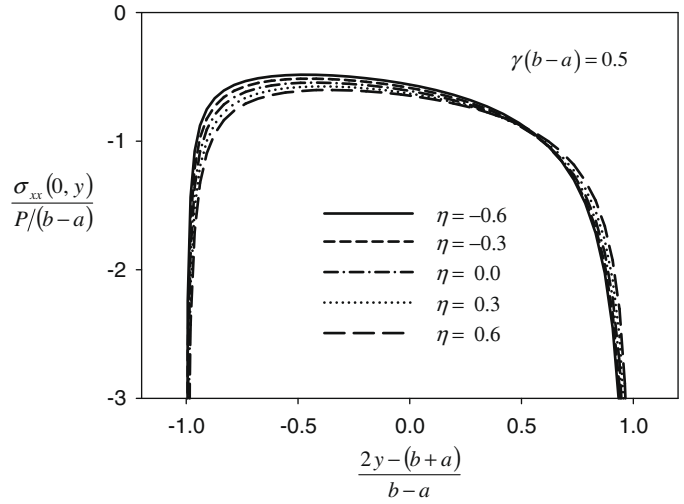

Fig. 7. Normalized contact stress distributions computed for various values of the coefficient of friction by considering a flat punch, $\gamma(b+a)=0$, $\kappa=1.8$, $\gamma(b-a)=0.5$.

In the finite element analyses of problems involving FGMs, two different methods are commonly used to take into account the smooth spatial variations of the material properties. Herein, we will refer to these methods as homogeneous finite element and graded finite element methods. In the graded finite element approach, the material properties are computed at each Gauss point of a finite element during the formation of an element stiffness matrix (Santare and Lambros, 2000). In the homogeneous finite element method however, the material properties are specified at the centroid of each finite element (Dag and Ilhan, 2008). Hence, the material distribution is uniform over a given finite element in the model. Previous studies show that with an appropriate degree of mesh refinement, it is possible to generate highly accurate numerical results using either method (Yildirim et al., 2005; Dag et al., 2007). In the present study, we employ the homogeneous finite element technique. As will be shown in the next section, a very good agreement is obtained between the results obtained by the analytical and computational methods which is indicative of the high levels of accuracy attained by these two separate techniques.

The finite element mesh used in the analysis of the flat punch problem is depicted in Fig. 4. This finite element mesh contains a total of 13,090 quadrilateral and triangular elements and 162 contact line elements. Note that for both flat and triangular punch problems identical mesh structures are utilized in the modeling of the graded elastic medium. In the finite element models, the rigid flat punch is represented by three rigid target elements whereas the rigid triangular punch is represented by two rigid target elements. As shown in Fig. 4, B, H and W, respectively, denote the width of the rigid punch, the height of the graded medium and the width of the graded medium. Since the graded elastic medium is modeled as an half-plane in the analytical solution, these dimensions are selected such that the boundaries of the elastic medium would have no influence on the contact stresses. Hence, B/W is taken as $1/20$ and H/W is set as $1/2$. Moreover, the finite element mesh density is increased significantly in the vicinity of the contact region so as to accurately capture the sharp variations of the stress components especially near the ends of the contact zone.

4. Numerical results

In this section, we present the numerical results generated by using the analytical and computational procedures whose details are provided in Sections 2 and 3. Before proceeding with the presentation of the numerical results, it is deemed useful to elaborate upon the nondimensional parameters used in the solutions of the flat and triangular punch problems. In both problems, the nonhomogeneity constant γ defines the degree of nonhomogeneity in the graded medium and the parameters a and b define the end points of the contact zone. Analytical formulation shows that instead of using these three separate parameters, it is possible to present the results in terms of two nondimensional parameters γa and γb. Another possibility is to use $\gamma(b-a)$ and $\gamma(b+a)$ instead of γa and γb. In all numerical results generated for the flat punch $\gamma(b+a)$ is fixed as zero and $\gamma(b-a)$ is taken as variable. Setting $\gamma(b+a)$ as zero implies that $a=-b$ hence the x-axis goes through center of the flat punch (see Fig. 2(a)). Unlike the flat punch problem, in the case of the triangular punch the size of the contact zone $(b-a)$ is a function of the applied force P. In the analyses conducted for the triangular punch, γb is taken as zero and γa is taken as the variable. Setting γb as zero implies that the x-axis goes through the right-end of the contact zone (see Fig. 2(b)). The normalized contact force corresponding to the specified values of γa and γb is then evaluated by utilizing Eq. (21). In the case of the flat

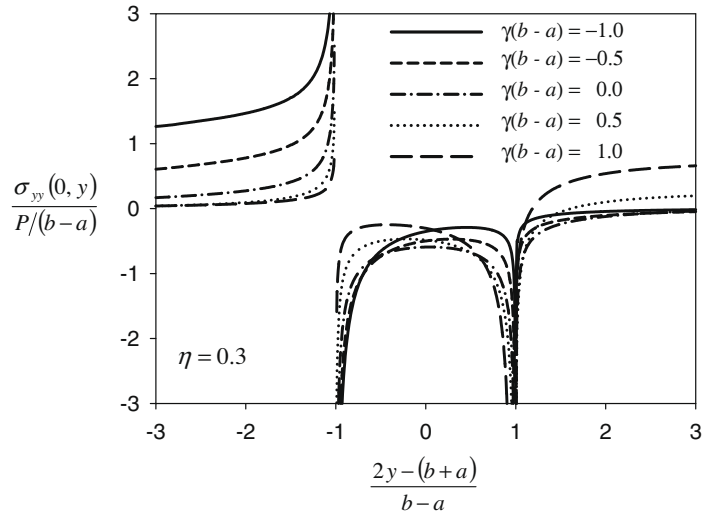

Fig. 8. Normalized lateral contact stress distributions computed for various values of the nondimensional nonhomogeneity constant $\gamma(b-a)$ by considering a flat punch, $\gamma(b+a)=0,\ \kappa=1.8,\ \eta=0.3$.

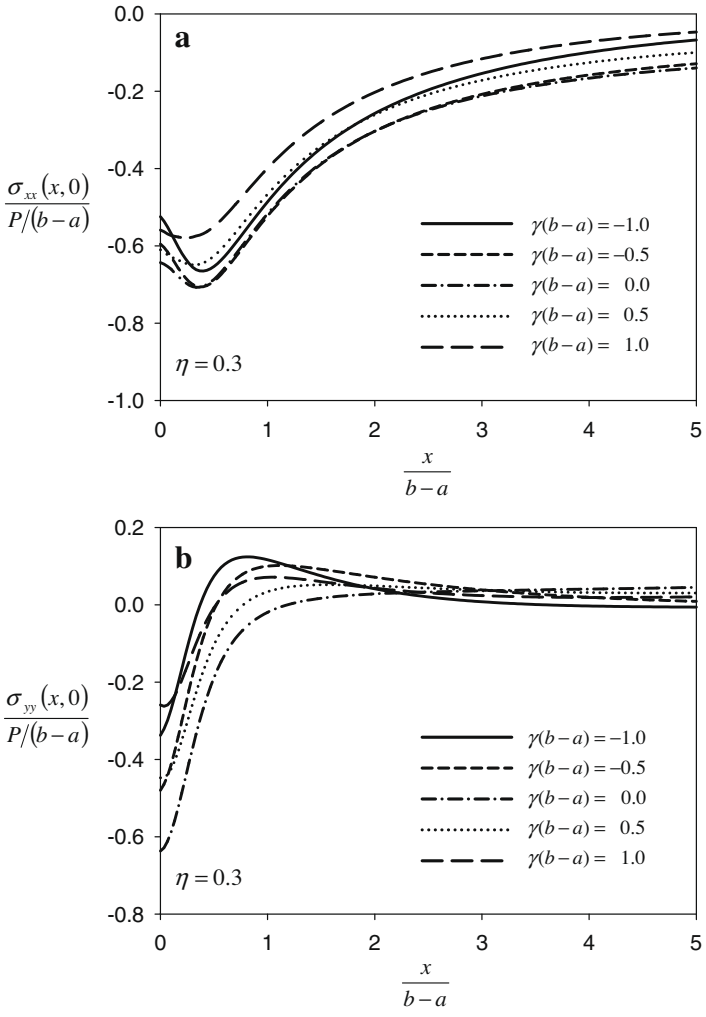

Fig. 9. Through-thickness distributions of the normalized stress components computed by considering a flat punch: (a) $\sigma_{xx}(x,0)/(P/(b-a))$; (b) $\sigma_{yy}(x,0)/(P/(b-a))$. $\eta=0.3,\ \gamma(b+a)=0,\ \kappa=1.8$.

punch such a calculation is not required since P and $(b-a)$ are independent.

The first set of results are provided in Figs. 5–10 and Table 1. These results are obtained by considering a flat punch. The second

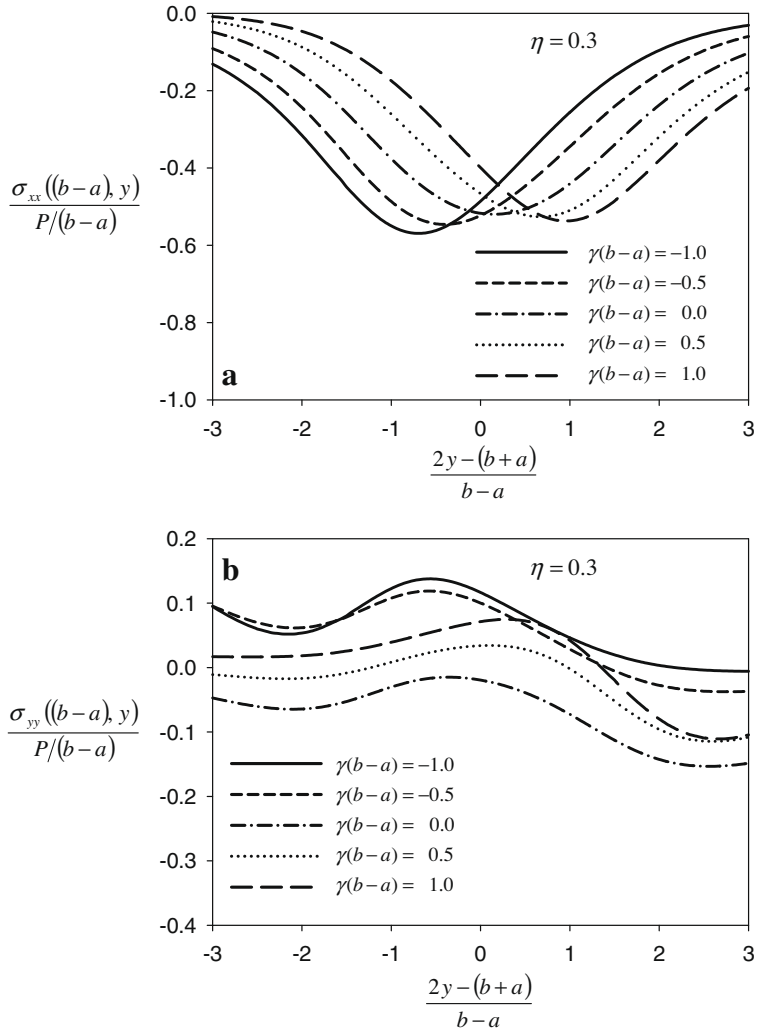

Fig. 10. Lateral distributions of the normalized stress components computed by considering a flat punch: (a) $\sigma_{xx}((b-a),y)/(P/(b-a))$; (b) $\sigma_{yy}((b-a),y)/(P/(b-a))$. $\eta = 0.3,\ \gamma(b+a) = 0,\ \kappa = 1.8$.

Table 1
Normalized contact stresses computed for various values of $\gamma(b-a)$, N and s by considering the flat punch, $\eta = 0.3,\ \gamma(b+a) = 0,\ \kappa = 1.8,\ s = (2y-(b+a))/(b-a)$.

	N	$\frac{\sigma_{xx}(0,s)}{P/(b-a)}$				
		$\gamma(b-a) = -1.0$	$\gamma(b-a) = -0.5$	$\gamma(b-a) = 0.0$	$\gamma(b-a) = 0.5$	$\gamma(b-a) = 1.0$
$s = -0.6$	1	−1.089	−1.016	−0.823	−0.597	−0.467
	2	−1.089	−1.014	−0.823	−0.598	−0.467
	4	−1.077	−1.012	−0.823	−0.600	−0.472
	8	−1.076	−1.011	−0.823	−0.600	−0.473
	12	−1.077	−1.012	−0.823	−0.600	−0.473
	16	−1.077	−1.011	−0.823	−0.600	−0.473
	20	−1.077	−1.011	−0.823	−0.600	−0.473
$s = 0$	1	−0.543	−0.592	−0.634	−0.623	−0.582
	2	−0.532	−0.585	−0.634	−0.631	−0.601
	4	−0.535	−0.586	−0.634	−0.630	−0.601
	8	−0.535	−0.586	−0.634	−0.630	−0.601
	12	−0.535	−0.586	−0.634	−0.630	−0.601
	16	−0.535	−0.586	−0.634	−0.630	−0.601
	20	−0.535	−0.586	−0.634	−0.630	−0.601
$s = 0.6$	1	−0.414	−0.528	−0.764	−0.995	−1.101
	2	−0.405	−0.526	−0.764	−0.999	−1.116
	4	−0.412	−0.527	−0.764	−0.998	−1.111
	8	−0.413	−0.528	−0.764	−0.997	−1.109
	12	−0.413	−0.527	−0.764	−0.998	−1.110
	16	−0.413	−0.527	−0.764	−0.998	−1.110
	20	−0.413	−0.527	−0.764	−0.998	−1.110

group of results, which are generated by considering a triangular punch, are given in Figs. 11–17 and Table 2. Fig. 5 shows the results on the normalized contact stress $\sigma_{xx}(0,y)/(P/(b-a))$ computed by considering a functionally graded medium loaded by a rigid flat punch. The normalized contact stress distributions evaluated through the analytical method and finite element analysis (FEA) are presented in this figure. The contact stress is plotted as a function of the normalized y-coordinate $\{2y-(b+a)\}/(b-a)$ which is equal to -1 for $y=a$ and 1 for $y=b$. The results are provided for five different values of the nondimensional nonhomogeneity constant $\gamma(b-a)$. The parameters that are fixed in the evaluation of these results are $\gamma(b+a)$, η and κ which are set as 0, 0.3 and 1.8, respectively. Note that a positive value for $\gamma(b-a)$ implies that the shear modulus increases in the lateral direction (y-direction) and a negative value implies that the shear modulus decreases in the lateral direction. The medium is homogeneous if the nondimensional parameter $\gamma(b-a)$ is equal to zero. It is seen that the results generated by the analytical and computational techniques are in very good agreement. The deformed shape of the finite element mesh of the region around the contact zone is depicted by Fig. 6.

Referring to Fig. 5, we observe that the contact stress $\sigma_{xx}(0,y)$ becomes singular at the end points of the contact zone $y=a$ and $y=b$. This is the expected result since the flat punch has sharp corners at both of these points. The influence of the nonhomogeneity constant on the normalized contact stress is rather significant. The contact stress goes through a maximum in the vicinity of the end

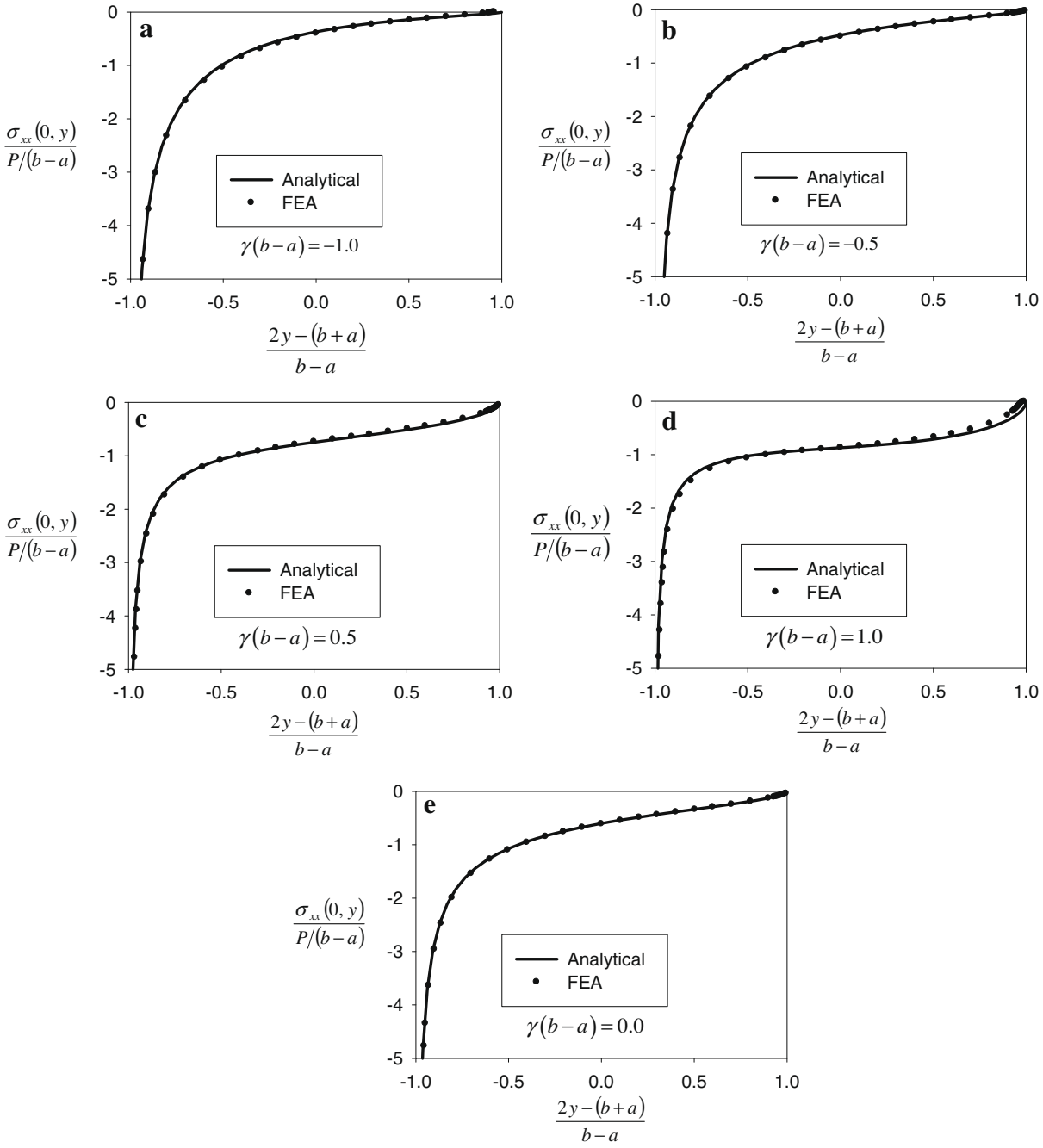

Fig. 11. Comparisons of the normalized contact stress distributions generated by considering a triangular punch: (a) $\gamma(b-a)=-1.0$; (b) $\gamma(b-a)=-0.5$; (c) $\gamma(b-a)=0.5$; (d) $\gamma(b-a)=1.0$; (e) $\gamma(b-a)=0.0$. $\eta=0.3,\ \gamma b=0,\ \kappa=1.8$.

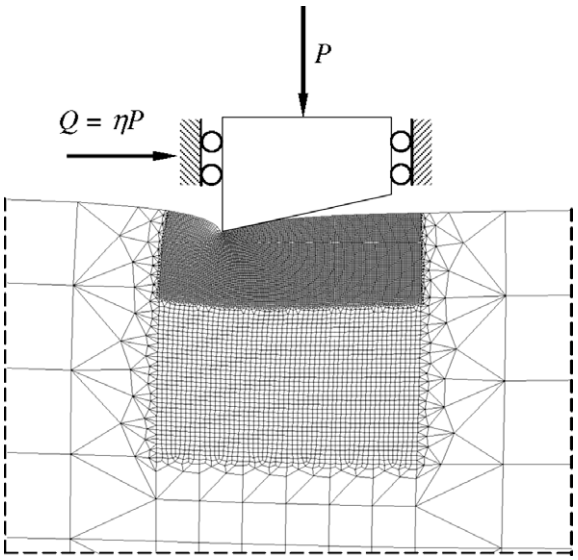

Fig. 12. Deformed shape of the finite element mesh of the region around the contact zone generated by considering a triangular punch, $\eta = 0.3,\ \gamma b = 0,\ \kappa = 1.8,\ \gamma(b-a) = 0.5$.

point $y = a$ if $\gamma(b-a) > 0$ and in the vicinity of the end point $y = b$ if $\gamma(b-a) < 0$. In other words, the contact stress slants towards the less stiff side for both $\gamma(b-a) > 0$ and $\gamma(b-a) < 0$. The normalized contact stress curve generated for $\gamma(b-a) = 0$ is also not symmetric about $y = 0$ due to the existence of the Coulomb friction in the contact zone. Note that once the normal contact stress $\sigma_{xx}(0,y)$ is computed, the shear stress $\sigma_{xy}(0,y)$ can be easily evaluated by using the Coulomb's law of dry friction $\sigma_{xy}(0,y) = \eta\sigma_{xx}(0,y)$.

Some numerical results are generated in order to examine the convergence characteristics of the analytical method described in Section 2. These results are computed by considering the flat punch and provided in Table 1. The table presents 15 cases for each of which the normalized contact stress is computed by using seven different values of *N*. Note that *N* is the upper limit of the *Nth* partial sum of the infinite series given by Eq. (26). The total number of collocation points used for Eq. (20) in the case of flat punch is also equal to *N*. As can be seen in Table 1, the results quickly converge as *N* is increased from 1 to 20. For each case, two-digit accuracy is achieved when $N = 4$ and three-digit accuracy is achieved when $N = 16$. All analytical results given in the present study are generated by taking *N* as 20.

In order to examine the influences of the coefficient of friction η and the nondimensional nonhomogeneity parameter $\gamma(b-a)$ on

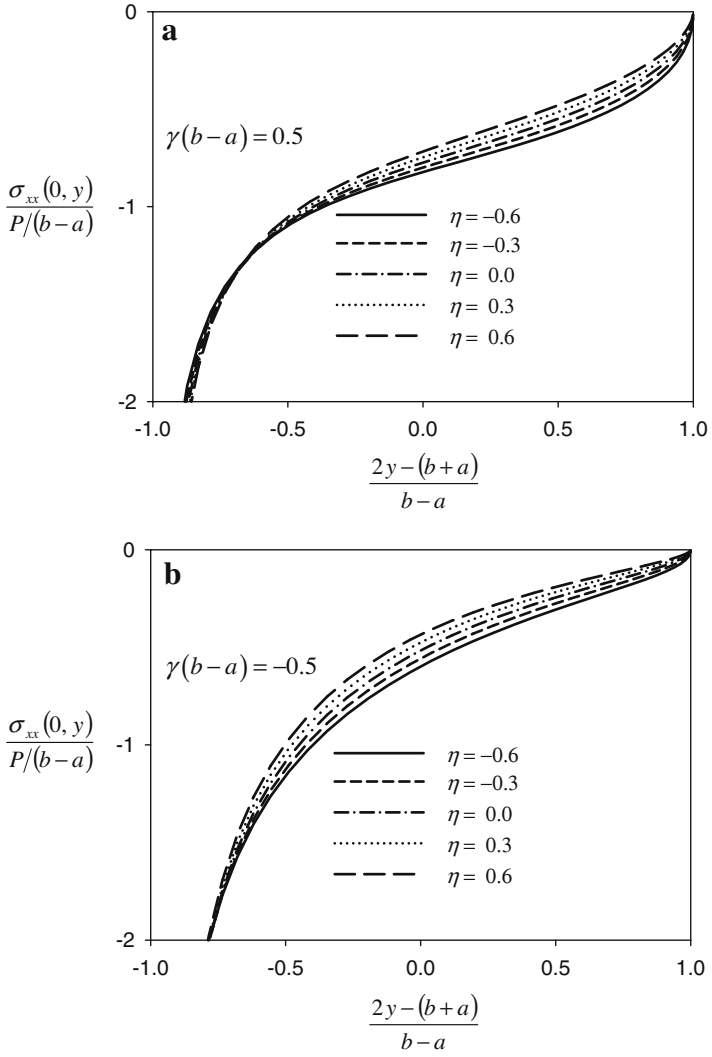

Fig. 13. Normalized contact stress distributions computed for various values of the coefficient of friction by considering a triangular punch: (a) $\gamma(b-a) = 0.5$; (b) $\gamma(b-a) = -0.5$. $\gamma b = 0,\ \kappa = 1.8$.

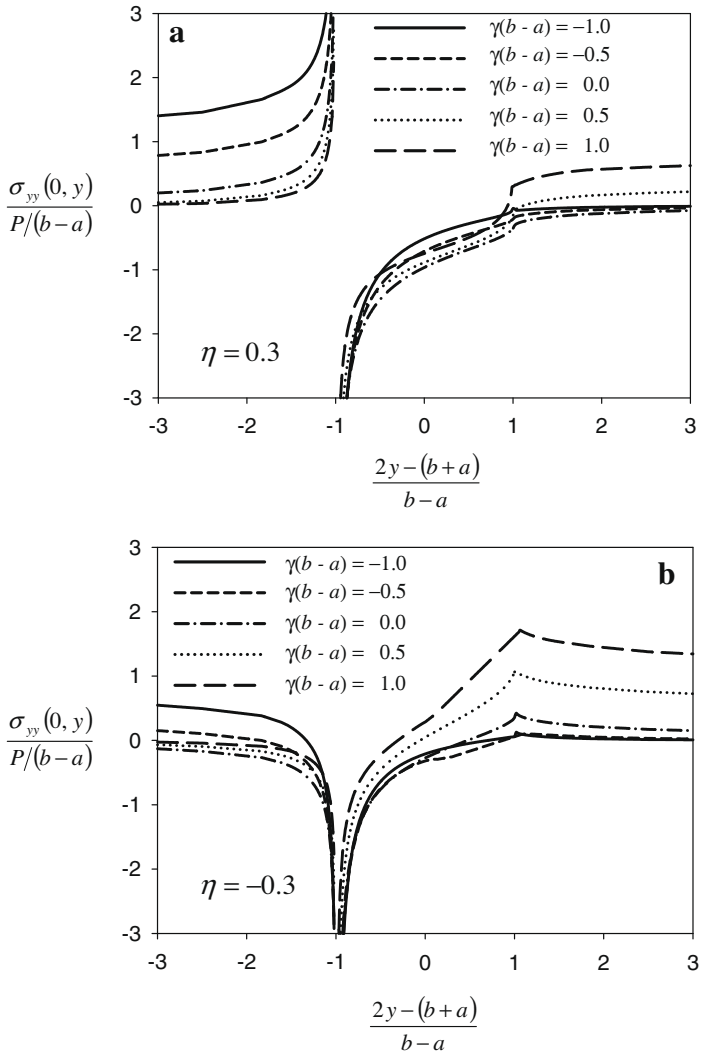

Fig. 14. Normalized lateral contact stress distributions computed for various values of the nondimensional nonhomogeneity constant $\gamma(b-a)$ by considering a triangular punch: (a) $\eta = 0.3$; (b) $\eta = -0.3$. $\gamma b = 0,\ \kappa = 1.8$.

the stress distributions, further results are generated for the flat punch by means of the developed finite element method. Fig. 7 shows the effect of the coefficient of friction on the normalized contact stress $\sigma_{xx}(0,y)/(P/(b-a))$. Note that the sign of the coefficient of friction is related to the direction of the friction force Q. When η is positive the friction force is acting in the positive y-direction whereas the friction force acts in the negative y-direction when η is negative. Since the contact stresses approach infinity at the ends of the contact zone, the curves generated for different values of η cannot be differentiated from each other near the end points. However away from the end points, the influence of the coefficient of friction is more visible. Examining Fig. 7, it can be seen that away from the end points of the contact zone the magnitude of the contact stress slightly increases as η is increased from -0.6 to 0.6.

One of the failure modes of brittle surfaces subjected to sliding frictional contact is known to be surface cracking in the wake of the trailing end of the contact track. The cracks that develop due to sliding frictional contact are generally referred to as herringbone cracks (Suresh et al., 1999) or as partial cone cracks (Lawn, 1993). The formation of the surface cracks in the wake of the trailing end of the contact zone is attributed to the development of tensile lateral stresses at the trailing end as the contacting agent slides on the free surface (Lawn, 1993). Hence, it is deemed important to provide some data regarding the influence of the nonhomogeneity parameter $\gamma(b-a)$ on the lateral contact stress evaluated at the free surface, i.e. on $\sigma_{yy}(0,y)$. Fig. 8 illustrates the effect of $\gamma(b-a)$ on the normalized lateral contact stress $\sigma_{yy}(0,y)/(P/(b-a))$ for $\eta = 0.3$. The results shown in this figure are generated by using the developed finite element analysis technique. Unlike the stress component $\sigma_{xx}(0,y)$, the lateral stress $\sigma_{yy}(0,y)$ is not zero in the region outside the contact zone ($y < a$ and $y > b$). It is seen that the lateral stress is positive and tends to ∞ near the trailing end of the contact zone ($y \to a^-$) regardless of the value of the nonhomogeneity constant. The lateral stress is negative in the contact zone ($a < y < b$) and approaches ($-\infty$) near the leading end of the contact ($y \to b^+$). The influence of the nonhomogeneity parameter on the lateral contact stress is rather significant especially near the trailing end of the contact. The magnitude of the tensile stress developed in the region near the trailing end decreases as the nonhomogeneity constant $\gamma(b-a)$ is increased from -1.0 to 1.0. Therefore, it can be inferred that, one way of suppressing herringbone crack formation could be the introduction of an elastic gradation such that the shear modulus increases in the direction of the applied friction force.

Some further finite element analyses are conducted by considering the flat punch, in order to examine the influence of the lateral gradation on the variations of subsurface stresses. The results of

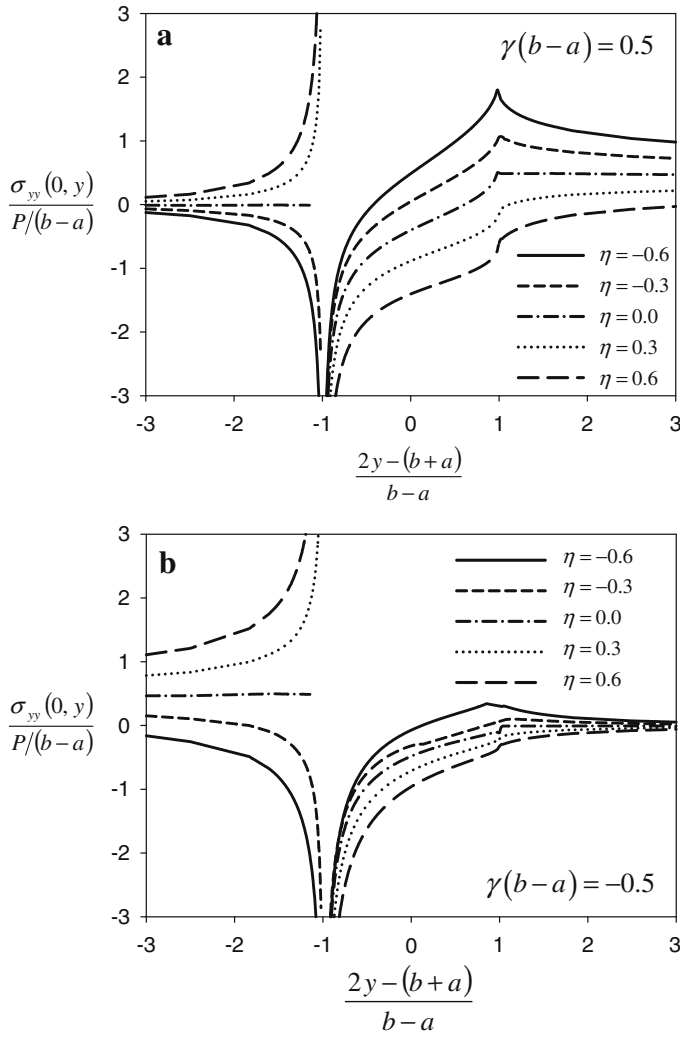

Fig. 15. Normalized lateral contact stress distributions computed for various values of the coefficient of friction by considering a triangular punch: (a) $\gamma(b-a)=0.5$; (b) $\gamma(b-a)=-0.5$. $\gamma b=0$, $\kappa=1.8$.

these analyses are given in Figs. 9 and 10. Fig. 9 shows the through-thickness distributions of the normalized stresses $\sigma_{xx}/(P/(b-a))$ and $\sigma_{yy}/(P/(b-a))$. The stress components are plotted as functions of the normalized thickness coordinate $x/(b-a)$ at a fixed value of $y=0$. For each of the stress components, the through-thickness variations are computed by considering five different values of $\gamma(b-a)$. It is seen that $\sigma_{xx}(x,0)$ goes through a minimum as the coordinate x is increased from zero. $\sigma_{xx}(x,0)$ is found to be always negative however $\sigma_{yy}(x,0)$ can be positive or negative depending on the values of $x/(b-a)$ and $\gamma(b-a)$. The largest $\sigma_{xx}(x,0)$ magnitudes are evaluated below the surface $(x>0)$ whereas the largest magnitudes for $\sigma_{yy}(x,0)$ are computed at the surface $(x=0)$. Except in a small zone near the surface, the normalized stresses in x-direction computed for $\gamma(b-a)=0$ and $\gamma(b-a)=-0.5$ are close to each other and magnitude-wise larger than those computed for the other three values of $\gamma(b-a)$. The variations of the normalized stresses in the lateral direction are displayed by Fig. 10. In this figure, the stresses are plotted as functions of the normalized y-coordinate $\{2y-(b+a)\}/(b-a)$ at a fixed value of $x=(b-a)$. Again, the results are provided for five different values of $\gamma(b-a)$. The normalized stresses in x-direction computed for all values of $\gamma(b-a)$ go through minima as the normalized coordinate is increased from -3 to 3. All the lateral stress curves on the other hand are observed to possess maxima. The influence of the nonhomogeneity constant $\gamma(b-a)$ on these subsurface stresses is found to be quite significant. The location of the point at which the minimum occurs for the normalized stress $\sigma_{xx}/(P/(b-a))$ shifts to right as $\gamma(b-a)$ increases. The normalized lateral stresses are negative for all values of $\{2y-(b+a)\}/(b-a)$ when $\gamma(b-a)$ is equal to 0. For the other $\gamma(b-a)$ values, the lateral stress is positive or negative depending on the normalized coordinate $\{2y-(b+a)\}/(b-a)$.

The results generated for a functionally graded medium loaded by a rigid triangular punch are presented in Figs. 11–17 and Table 2. The geometry of the triangular punch is depicted by Fig. 2(b). In the triangular punch problem the length of the contact region $(b-a)$ is dependent upon the applied normal force P. In the analytical solution of the triangular punch problem, the parameters γa and γb are specified and the corresponding normalized contact force is determined by Eq. (21). In all parametric analyses conducted for the triangular punch, γb is fixed as zero and γa is taken as the variable quantity. In the figures, the curves are presented as functions of the parameter $\gamma(b-a)$ in order to have consistent styles of presentations for the flat and triangular punch problems. Table 2 tabulates the normalized forces $P/\{\mu_0\tan(\theta)(b-a)\}$ computed by using the analytical technique for various values of the coefficient of friction η and the nonhomogeneity constant $\gamma(b-a)$. In the finite element analyses, the normalized contact force values given in Table 2 are used as inputs and resulting values of γb are checked to see whether the condition $\gamma b=0$ is satisfied.

The comparisons of the normalized contact stresses computed by using the analytical and finite element methods are provided in Fig. 11. The results are generated for five different values of the nondimensional nonhomogeneity constant $\gamma(b-a)$. The parameters that are fixed in the evaluation of these results are γb, η and κ which are set as 0, 0.3 and 1.8, respectively. It is seen that the normalized contact stress tends to infinity near $y=a$ and is equal to zero at the end point $y=b$. This is due to the fact that there is a sharp corner at $y=a$ and smooth contact at $y=b$. In all cases, the results generated by the analytical and finite element methods are seen to be in very good agreement. The deformed shape of the finite element mesh of the region around the contact zone is provided in Fig. 12.

Fig. 13 shows the plots of the normalized contact stress $\sigma_{xx}(0,y)/(P/(b-a))$ as functions of the coefficient of friction η. The results presented in these figures and in Figs. 14–17 are generated by using the developed finite element analysis technique. Examining Fig. 13, it can be observed that, away from the sharp corner of the triangular punch, the normalized contact stress increases as the coefficient of friction is increased from -0.6 to 0.6. This trend is seen to be valid for both $\gamma(b-a)=0.5$ and $\gamma(b-a)=-0.5$. In Figs. 14 and 15, the influences of the nondimensional nonhomogeneity parameter and the coefficient of friction on the normalized lateral contact stress $\sigma_{yy}(0,y)/(P/(b-a))$ are presented. Fig. 14(a) depicts the behavior of the lateral contact stress when the friction force acts in the positive y-direction. The coefficient of friction is taken as 0.3. The plots in this figure are generated for five different values of $\gamma(b-a)$. It is clearly seen that for all values of $\gamma(b-a)$, the lateral stress is positive and tends to infinity near the trailing end of the contact $(y\to a^-)$. The normalized lateral stress near the trailing end is found to be a decreasing function of the nonhomogeneity parameter $\gamma(b-a)$. In Fig. 14(b), the direction of the friction force is reversed by taking η as -0.3. When the direction of the friction force is reversed, the trailing end of the contact becomes $y=b$ and the leading end becomes $y=a$. For this case, albeit bounded, the lateral contact stress near the trailing end is still positive. The normalized lateral stress near the trailing end is found to be an increasing function of the nonhomogeneity parameter $\gamma(b-a)$ when η is negative. Therefore, an important conclusion can be drawn regarding the influence of the elastic gra-

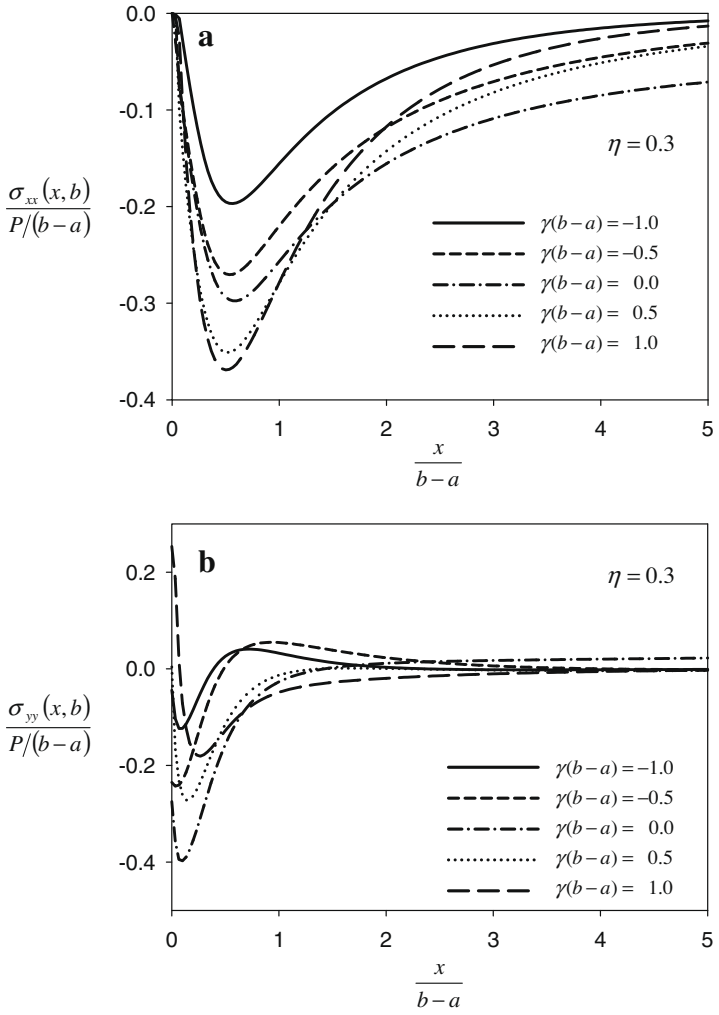

Fig. 16. Through-thickness distributions of the normalized stress components computed by considering a triangular punch: (a) $\sigma_{xx}(x,b)/(P/(b-a))$; (b) $\sigma_{yy}(x,b)/(P/(b-a))$. $\eta = 0.3,\ \gamma b = 0,\ \kappa = 1.8$.

dation in the lateral direction. The normalized lateral contact stresses near the trailing end calculated for a medium that possesses a shear modulus increasing in the direction of the friction force will be smaller than those calculated for a homogeneous medium. This observation is seen to be valid for both flat and triangular punch problems. In the present study, the coefficient of friction between the rigid punch and the laterally graded elastic medium is assumed to be a constant. In general, the coefficient of friction for two elastic solids in contact is known to be dependent upon the elastic properties of the material pair (Halling, 1976). Since, the shear modulus is taken as a function of the lateral coordinate y in the current study, the coefficient of friction could also be a function of y for $a \leqslant y \leqslant b$. As a result, the distribution profile of the friction coefficient within the contact zone may also have a bearing on the contact stresses. However, the main trends presented in this section are expected to be similar to those that would be observed if the variation in the coefficient of friction were taken into account.

Each of Figs. 15(a) and (b) displays the plots of the normalized lateral stress for five different values of the coefficient of friction η. The nondimensional nonhomogeneity parameter $\gamma(b-a)$ is fixed as 0.5 in Fig. 15(a) and as -0.5 in Fig. 15(b). We again note that a change in the sign of the coefficient of friction corresponds to a reversal in the direction of the applied friction force. Examining both figures it is seen that as a general trend, the lateral stress is positive near the trailing end and negative near the leading end. Furthermore, the magnitude of the normalized lateral stress in the region near the trailing end increases as the absolute value of the coefficient of friction is increased. In other words, a larger friction force leads to larger normalized lateral tensile stresses in the region near the trailing end of the contact zone.

The results generated by means of the finite element method to examine the variations of the subsurface stresses induced by the triangular punch are given in Figs. 16 and 17. Fig. 16 shows the normalized stresses $\sigma_{xx}/(P/(b-a))$ and $\sigma_{yy}/(P/(b-a))$ plotted as functions of the normalized thickness coordinate $x/(b-a)$ at a fixed value of $y = b$. For both stress components, the results are given for five different values of the nonhomogeneity constant $\gamma(b-a)$. The stresses are seen to go through minima as the normalized coordinate $x/(b-a)$ is increased from zero. The minimum value calculated for $\sigma_{xx}(x,b)/(P/(b-a))$ decreases whereas the minimum value calculated for $\sigma_{yy}(x,b)/(P/(b-a))$ itself goes through a minimum as the nonhomogeneity parameter $\gamma(b-a)$ is increased from -1 to 1. The variations of the normalized subsurface stresses $\sigma_{xx}((b-a),y)/(P/(b-a))$ and $\sigma_{yy}((b-a),y)/(P/(b-a))$ are illustrated by Fig. 17. In this figure, the stress components are plotted as functions of the normalized coordinate $\{2y-(b+a)\}/(b-a)$ and $\gamma(b-a)$. The curves for $\sigma_{xx}((b-a),y)/(P/(b-a))$ go through minima as the normalized coordinate is increased from -3 to 3. The curves generated for the normalized lateral stress on the other hand, possess points of maxima. The effect

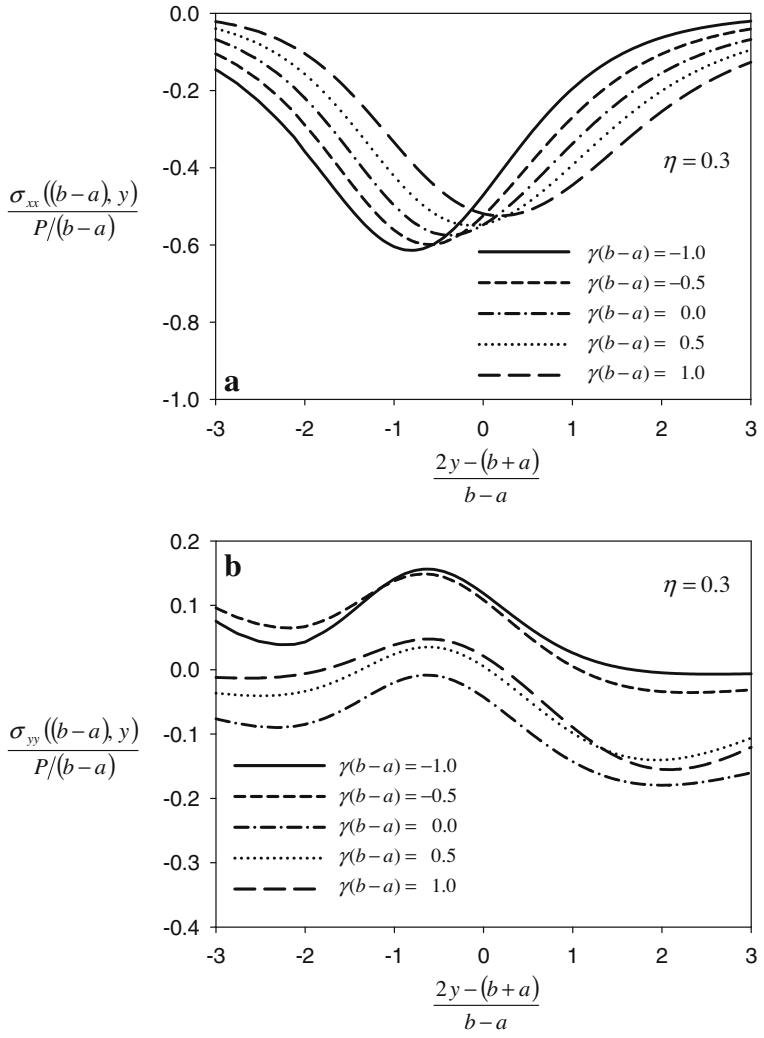

Fig. 17. Lateral distributions of the normalized stress components computed by considering a triangular punch: (a) $\sigma_{xx}((b-a),y)/(P/(b-a))$; (b) $\sigma_{yy}((b-a),y)/(P/(b-a))$. $\eta = 0.3,\ \gamma b = 0,\ \kappa = 1.8$.

Table 2
Normalized forces computed for various values of the coefficient of friction η and the nondimensional nonhomogeneity constant $\gamma(b-a)$ by considering the triangular punch, $\gamma b = 0,\ \kappa = 1.8$.

η	$\frac{P}{\mu_0 \tan(\theta)(b-a)}$				
	$\gamma(b-a) = -1.0$	$\gamma(b-a) = -0.5$	$\gamma(b-a) = 0.0$	$\gamma(b-a) = 0.5$	$\gamma(b-a) = 1.0$
−0.6	6.090	3.683	2.002	1.270	0.988
−0.3	6.235	3.891	2.122	1.338	1.043
0.0	6.298	4.081	2.244	1.408	1.101
0.3	6.278	4.247	2.366	1.480	1.160
0.6	6.188	4.383	2.487	1.551	1.222

of the lateral gradation on the subsurface stresses is found to be significant. The point where the minimum occurs for $\sigma_{xx}((b-a), y)/(P/(b-a))$ shifts to right as $\gamma(b-a)$ increases. The normalized lateral stress is negative for all values $\{2y-(b+a)\}/(b-a)$ when the nonhomogeneity parameter $\gamma(b-a)$ is equal to zero. For the remaining values of $\gamma(b-a)$, the lateral stresses can be positive or negative depending on the value of $\{2y-(b+a)\}/(b-a)$.

5. Conclusions

This article presents analytical and computational methods for the computation of the contact stress distributions in laterally graded materials that are subjected to sliding frictional contact. The analytical method is developed by deriving a singular integral equation whereas the computational method is based on a finite element analysis technique. The comparisons provided in Section 4 indicate that the contact stress distributions obtained by these two separate methods are in very good agreement which is indicative of the high levels of accuracy achieved by means of these methods. One of the general conclusions that can be drawn by examining the analytical formulation presented in Section 2 is that, the singular behavior of the contact stress that develops in laterally graded materials is exactly same as that obtained for homogeneous materials. The strengths of the singularities derived for laterally

graded materials are not functions of the nonhomogeneity constant but functions of the Poisson's ratio and the coefficient of friction.

Numerical results are provided in Section 4 by considering both complete and incomplete contact problems. In the complete contact problem, the graded medium is assumed to be loaded through a rigid flat punch. For the flat punch, the stresses are singular at both ends of the contact zone and the contact force per unit length P is independent of the length of the contact region. In the incomplete contact problem however, a loading due to a rigid triangular punch is considered. The magnitude of the contact force per unit length for a triangular punch is a function of the length of the contact zone. In the finite element analyses of both flat and triangular punch problems, homogeneous finite elements are utilized and the material properties are specified at the centroid of each finite element during construction of the element stiffness matrices. The close agreement between the results obtained by the analytical and computational methods demonstrates the effectiveness of the homogeneous finite element approach.

Detailed parametric analyses are conducted in order to assess the influences of the nonhomogeneity parameter $\gamma(b-a)$ and the coefficient of friction η on the contact stresses. The influences of both of these parameters especially on the lateral contact stress $\sigma_{yy}(0,y)$ are found to be highly significant. The magnitude of the lateral contact stress is known to be one of the driving forces that affect the formation of herringbone cracks at brittle surfaces subjected to sliding frictional contact. It is shown that for both flat and triangular punch problems, the normalized lateral stress near the trailing end computed for a medium that possesses a shear modulus increasing in the direction of the friction force is smaller than that computed for a homogeneous medium. Hence, by suitably introducing a lateral elastic gradation into a contacting surface it could be possible to improve the resistance to damage that results from sliding frictional contact.

One of the basic assumptions of the present study is that the coefficient of friction between the rigid punch and the laterally graded elastic medium is a constant. In the case of an elastic contact, the coefficient of friction in general depends on the elastic properties of the contacting materials (Halling, 1976). Accordingly, it could be argued that the coefficient of friction for the contact between the rigid punch and the laterally graded elastic medium is also a function of the lateral coordinate y. The variation profile of the coefficient of friction may also influence contact stress distributions. Even so, the results reported in the present study are expected not to be very different from those that would be computed under the assumption that the coefficient of friction is variable.

Acknowledgement

This work was partially supported by the Scientific and Technical Research Council of Turkey (TUBITAK) through Grant MAG-107M053.

Appendix A. Expressions of the functions $k_1(y,t)$ and $k_2(y,t)$

In this appendix, we provide the expressions of the functions $k_1(y,t)$ and $k_2(y,t)$ that appear in Eq. (15). These functions are defined as follows:

$$k_1(y,t)=h_{11}(y,t)+h_{12}(y,t),\quad k_2(y,t)=h_{13}(y,t)+h_{14}(y,t). \tag{A.1}$$

$h_{11}(y,t)$, $h_{12}(y,t)$, $h_{13}(y,t)$ and $h_{14}(y,t)$ are given by

$$h_{11}(y,t)=\int_0^{A_{11}}K_{11}(\rho)\cos(\rho(y-t))d\rho+\int_{A_{11}}^{\infty}\left\{\frac{a_1}{\rho}+\frac{a_3}{\rho^3}+\frac{a_5}{\rho^5}+\frac{a_7}{\rho^7}\right\}\cos(\rho(y-t))d\rho, \tag{A.2}$$

$$h_{12}(y,t)=\int_0^{A_{12}}\{K_{12}(\rho)-\frac{1+\kappa}{2}\}\sin(\rho(y-t))d\rho+\int_{A_{12}}^{\infty}\left\{\frac{b_2}{\rho^2}+\frac{b_4}{\rho^4}+\frac{b_6}{\rho^6}\right\}\sin(\rho(y-t))d\rho, \tag{A.3}$$

$$h_{13}(y,t)=\int_0^{A_{13}}\{K_{13}(\rho)-\frac{1-\kappa}{2}\}\cos(\rho(y-t))d\rho+\int_{A_{13}}^{\infty}\left\{\frac{c_2}{\rho^2}+\frac{c_4}{\rho^4}+\frac{c_6}{\rho^6}\right\}\cos(\rho(y-t))d\rho, \tag{A.4}$$

$$h_{14}(y,t)=\int_0^{A_{14}}K_{14}(\rho)\sin(\rho(y-t))d\rho+\int_{A_{14}}^{\infty}\left\{\frac{d_1}{\rho}+\frac{d_3}{\rho^3}+\frac{d_5}{\rho^5}+\frac{d_7}{\rho^7}\right\}\sin(\rho(y-t))d\rho, \tag{A.5}$$

where A_{jk} are integration cut-off points used for the improper integrals. The constants a_j, b_j, c_j and d_j are determined through asymptotic analyses and provided in Appendix B. The functions $K_{jk}(\rho)$ are expressed in the following form:

$$K_{11}(\rho)=H_{11}(\rho)+H_{11}(-\rho), \tag{A.6}$$

$$K_{12}(\rho)=i[H_{11}(\rho)-H_{11}(-\rho)], \tag{A.7}$$

$$K_{13}(\rho)=H_{12}(\rho)+H_{12}(-\rho), \tag{A.8}$$

$$K_{14}(\rho)=i[H_{12}(\rho)-H_{12}(-\rho)]. \tag{A.9}$$

$H_{11}(\rho)$ and $H_{12}(\rho)$ are given as

$$H_{11}(\rho)=i\rho(\phi_1(\rho)+\phi_2(\rho)),\quad H_{12}(\rho)=i\rho(\lambda_1(\rho)+\lambda_2(\rho)), \tag{A.10}$$

where $\phi_j(\rho)$ and $\lambda_j(\rho)$ $(j=1,2)$ are defined by Eq. (14). Note that the first integrals in the right hand sides of Eqs. (A.2)–(A.5) are calculated numerically whereas the second integrals are evaluated in closed-form.

Appendix B. Constants obtained through asymptotic expansions

As shown by Eqs. (A.2)–(A.5), the expressions of $h_{11}(y,t)$, $h_{12}(y,t)$, $h_{13}(y,t)$ and $h_{14}(y,t)$, respectively, contain the constants, a_j, b_j, c_j and d_j. These constants are obtained through asymptotic analyses and their expressions are provided below:

$$a_1=-\frac{\gamma(2\kappa^2-3\kappa-5)}{4}, \tag{B.1}$$

$$a_3=\frac{\gamma^3(\kappa^4-5\kappa^3+9\kappa^2-3\kappa-13)}{8}, \tag{B.2}$$

$$a_5=-\frac{\gamma^5(\kappa^7-6\kappa^6+13\kappa^5-12\kappa^4+\kappa^3+30\kappa^2-60\kappa-54)}{32(\kappa+1)}, \tag{B.3}$$

$$a_7=\frac{\gamma^7(\kappa^{10}-7\kappa^9+18\kappa^8-18\kappa^7-6\kappa^6+30\kappa^5-26\kappa^4+98\kappa^3-114\kappa^2-451\kappa-216)}{128(\kappa+1)^2}, \tag{B.4}$$

$$b_2=-\frac{\gamma^2(\kappa^3-4\kappa^2+2\kappa+6)}{4}, \tag{B.5}$$

$$b_4=\frac{\gamma^4(\kappa^6-5\kappa^5+8\kappa^4-4\kappa^3-15\kappa^2+30\kappa+26)}{16(\kappa+1)}, \tag{B.6}$$

$$b_6=-\frac{\gamma^6(\kappa^9-6\kappa^8+12\kappa^7-6\kappa^6-12\kappa^5+18\kappa^4-56\kappa^3+53\kappa^2+221\kappa+105)}{64(\kappa+1)^2}, \tag{B.7}$$

$$c_2=\frac{\gamma^2(\kappa^3-2\kappa^2-1)}{4}, \tag{B.8}$$

$$c_4=-\frac{\gamma^4(\kappa^5-4\kappa^4+6\kappa^3-4\kappa^2-3\kappa-4)}{16}, \tag{B.9}$$

$$c_6=\frac{\gamma^6(\kappa^7-6\kappa^6+15\kappa^5-20\kappa^4+15\kappa^3-6\kappa^2-15\kappa-16)}{64}, \tag{B.10}$$

$$d_1=-\frac{\gamma(2\kappa^2-3\kappa-1)}{4}, \tag{B.11}$$

$$d_3=\frac{\gamma^3(\kappa^4-3\kappa^3+3\kappa^2-3\kappa-2)}{8}, \tag{B.12}$$

$$d_5 = -\frac{\gamma^5(\kappa^6 - 5\kappa^5 + 10\kappa^4 - 10\kappa^3 + 5\kappa^2 - 9\kappa - 8)}{32}, \quad \text{(B.13)}$$

$$d_7 = \frac{\gamma^7(\kappa^8 - 7\kappa^7 + 21\kappa^6 - 35\kappa^5 + 35\kappa^4 - 21\kappa^3 + 7\kappa^2 - 33\kappa - 32)}{128}. \quad \text{(B.14)}$$

References

ANSYS, 1997. ANSYS Basic Analysis Procedures Guide, Release 5.4. ANSYS Inc., Canonsburg, PA, USA, 1997.

Cannillo, V., Lusvarghi, L., Siligardi, C., Sola, A., 2007. Prediction of the elastic properties profile in glass–alumina functionally graded materials. Journal of the European Ceramic Society 27, 2393–2400.

Choi, H.J., Paulino, G.H., 2008. Thermoelastic contact mechanics for a flat punch sliding over a graded coating/substrate system with frictional heat generation. Journal of the Mechanics and Physics of Solids 56, 1673–1692.

Dag, S., Erdogan, F., 2002a. A surface crack in a graded medium loaded by a sliding rigid stamp. Engineering Fracture Mechanics 69, 1729–1751.

Dag, S., Erdogan, F., 2002b. A surface crack in a graded medium under general loading conditions. Journal of Applied Mechanics – Transactions of the ASME 69, 580–588.

Dag, S., Yildirim, B., Sarikaya, D., 2007. Mixed-mode fracture analysis of orthotropic functionally graded materials under mechanical and thermal loads. International Journal of Solids and Structures 44, 7816–7840.

Dag, S., Ilhan, K.A., 2008. Mixed-mode fracture analysis of orthotropic functionally graded material coatings using analytical and computational methods. Journal of Applied Mechanics – Transactions of the ASME 75, 051104.

Erdogan, F., 1978. Mixed boundary value problems in mechanics. In: Nemat-Nasser, S. (Ed.), Mechanics Today, vol. 4. Pergamon Press, New York, pp. 1–86.

Ganesh, V.K., Ramakrishna, K., Ghista, D.N., 2005. Biomechanics of bone-fracture fixation by stiffness-graded plates in comparison with stainless-steel plates. Biomedical Engineering Online 4, 46.

Giannakopoulos, A.E., Pallot, P., 2000. Two-dimensional contact analysis of elastic graded materials. Journal of the Mechanics and Physics of Solids 48, 1596–1631.

Guler, M.A., Erdogan, F., 2004. Contact mechanics of graded coatings. International Journal of Solids and Structures 41, 3865–3889.

Guler, M.A., Erdogan, F., 2006. Contact mechanics of two deformable solids with graded coatings. Mechanics of Materials 38, 633–647.

Guler, M.A., Erdogan, F., 2007. The frictional sliding contact problems of rigid parabolic and cylindrical stamps on graded coatings. International Journal of Mechanical Sciences 49, 161–182.

Guler, M.A., 2008. Mechanical modeling of thin films and cover plates bonded to graded substrates. Journal of Applied Mechanics – Transactions of the ASME 75, 051105.

Halling, J., 1976. Introduction to Tribology. Wykeham Publications, London, UK.

Hills, D.A., Nowell, D., 1994. Mechanics of Fretting Fatigue. Kluwer Academic Publishers, Dordrecht, The Netherlands.

Jitcharoen, J., Padture, N.P., Giannakopoulos, A.E., Suresh, S., 1998. Hertzian-crack suppression in ceramics with elastic-modulus-graded surfaces. Journal of the American Ceramic Society 81, 2301–2308.

Ke, L.L., Wang, Y.S., 2006. Two-dimensional contact mechanics of functionally graded materials with arbitrary variations of material properties. International Journal of Solids and Structures 43, 5779–5798.

Ke, L.L., Wang, Y.S., 2007a. Two-dimensional sliding frictional contact of functionally graded materials. European Journal of Mechanics A – Solids 26, 171–188.

Ke, L.L., Wang, Y.S., 2007b. Fretting contact with finite friction of a functionally graded coating with arbitrarily varying elastic modulus. Part 1: Normal loading. Journal of Strain Analysis for Engineering Design 42, 293–304.

Ke, L.L., Wang, Y.S., 2007c. Fretting contact with finite friction of a functionally graded coating with arbitrarily varying elastic modulus. Part 2: Tangential loading. Journal of Strain Analysis for Engineering Design 42, 305–313.

Khor, K.A., Gu, Y., 2000. Thermal properties of plasma-sprayed functionally graded thermal barrier coatings. Thin Solid Films 372, 104–113.

Lawn, B., 1993. Fracture of Brittle Solids. Cambridge University Press, Cambridge, UK.

Mishina, H., Inumaru, Y., Kaitoku, K., 2008. Fabrication of ZrO_2/AISI316L functionally graded materials for joint prostheses. Materials Science & Engineering A 475, 141–147.

Nomura, T., Moriguchi, H., Tsuda, K., Isobe, K., Ikegaya, A., Moriyama, K., 1999. Material design method for the functionally graded cemented carbide tool. International Journal of Refractory Metals & Hard Materials 17, 397–404.

Ozatag, A.C., 2003. Contact mechanics of a graded surface with elastic gradation in lateral direction. MS Thesis, Middle East Technical University, Ankara, Turkey.

Park, C.W., Lee, B.S., Walker, J.K., Choi, W.Y., 2000. A new processing method for fabrication of cylindrical objects with radially varying properties. Industrial & Engineering Chemistry Research 39, 79–83.

Pender, D.C., Padture, N.P., Giannakopoulos, A.E., Suresh, S., 2001a. Gradients in elastic modulus for improved contact-damage resistance. Part I: The silicon nitride–oxynitride glass system. Acta Materialia 49, 3255–3262.

Pender, D.C., Thompson, S.C., Padture, N.P., Giannakopoulos, A.E., Suresh, S., 2001b. Gradients in elastic modulus for improved contact-damage resistance. Part II: The silicon nitride–silicon carbide system. Acta Materialia 49, 3263–3268.

Santare, M.H., Lambros, J., 2000. Use of graded finite elements to model the behavior of nonhomogeneous materials. Journal of Applied Mechanics – Transactions of the ASME 67, 819–822.

Suresh, S., Olsson, M., Giannakopoulos, A.E., Padture, N.P., Jitcharoen, J., 1999. Engineering the resistance to sliding-contact damage through controlled gradients in elastic properties at contact surfaces. Acta Materialia 47, 3915–3926.

Yang, J., Xiang, H.J., 2007. Thermo–electro-mechanical characteristics of functionally graded piezoelectric actuators. Smart Materials and Structures 16, 784–797.

Yang, J., Ke, L.L., 2008. Two dimensional contact problem for a coating-graded layer–substrate structure under a rigid cylindrical punch. International Journal of Mechanical Sciences 50, 985–994.

Yildirim, B., Dag, S., Erdogan, F., 2005. Three dimensional fracture analysis of FGM coatings under thermomechanical loading. International Journal of Fracture 132, 371–397.

Yue, T.M., Li, T., 2008. Laser cladding of Ni/Cu/Al functionally graded coating on magnesium substrate. Surface & Coatings Technology 202, 3043–3049.

Zhang, J., Sun, K., Wang, J., Tian, B., Wang, H., Yin, Y., 2008. Sliding wear behavior of plasma sprayed Fe_3Al—Al_2O_3 graded coatings. Thin Solid Films 516, 5681–5685.